8th International Conference on Fracture Mechanics of Concrete and Concrete Structures

FraMCoS-8

University of Castilla La-Mancha

March 10-14, 2013 / Toledo - Spain

PEEL STRENGTH TESTING OF FRP APPLIED TO CLAY BRICKS

Matteo Panizza, Enrico Garbin, Maria Rosa Valluzzi, Claudio Modena

University of Padua – Italy

Department of Civil, Architectural and Environmental Engineering

FRP strengthening of masonry arches

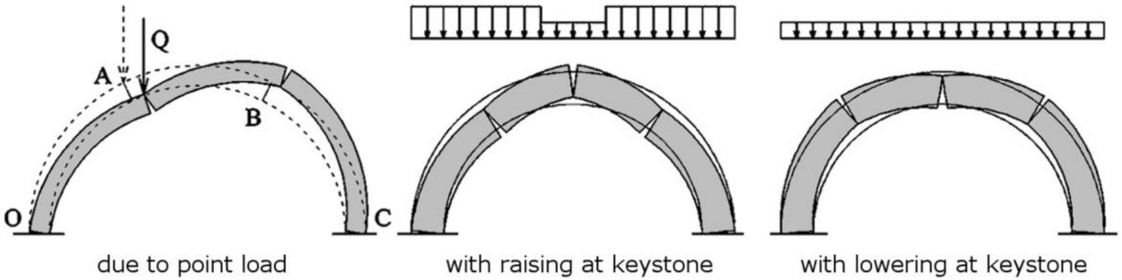

Examples of collapse mechanisms of unreinforced arches

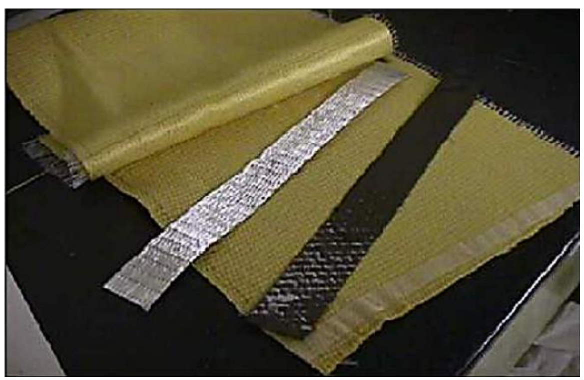

Externally Bonded FRP textiles (carbon, glass, aramid, basalt…)

Intrados application

Extrados application

Local failure mechanisms of reinforced structures

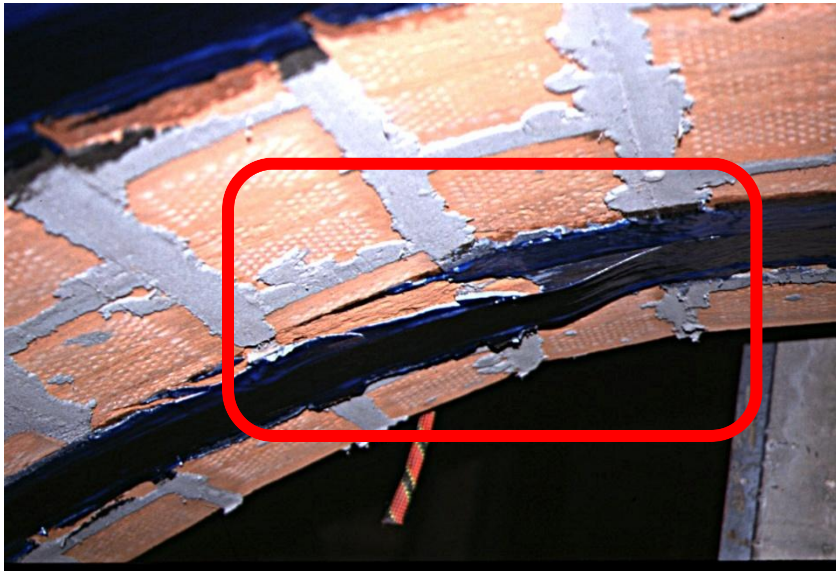

INTRADOS REINFORCEMENT

detachment of the reinforcement from the support, due to normal stresses related to the curved shape of the FRP itself, which is working under tension

EXTRADOS REINFORCEMENT

sliding on a mortar joint, due to excessive shear force, close to the springer opposite to the loading point in the case of asymmetric configuration

Shear failure – extrados reinforcement

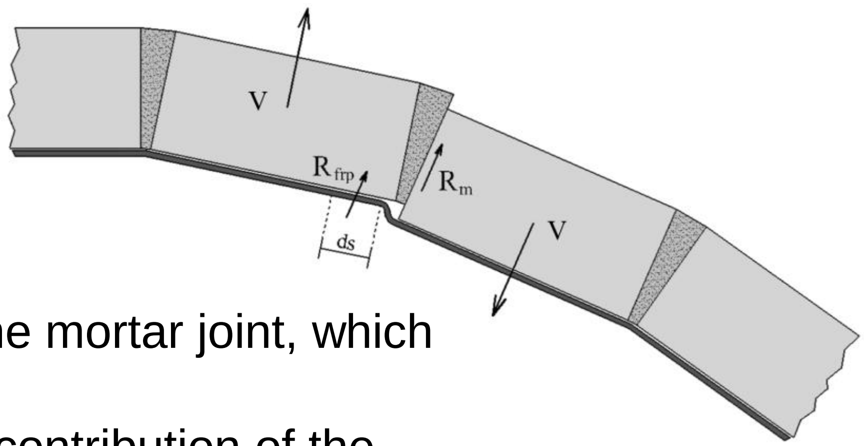

Available model: Coulomb-like strength of the mortar joint, which consider only the masonry contribution.
Starting point: trying to measure a possible contribution of the reinforcement to the resistance mechanism of the joint.

Investigation method: performing of fourteen V-shape Peel Tests on solid clay bricks with EB CFRP.
Test set-up was derived from similar set-ups developed for reinforced concrete (Wu et al. 2005, Dai & Ueda 2007)
Tests were aimed at isolating the reinforcement contribution

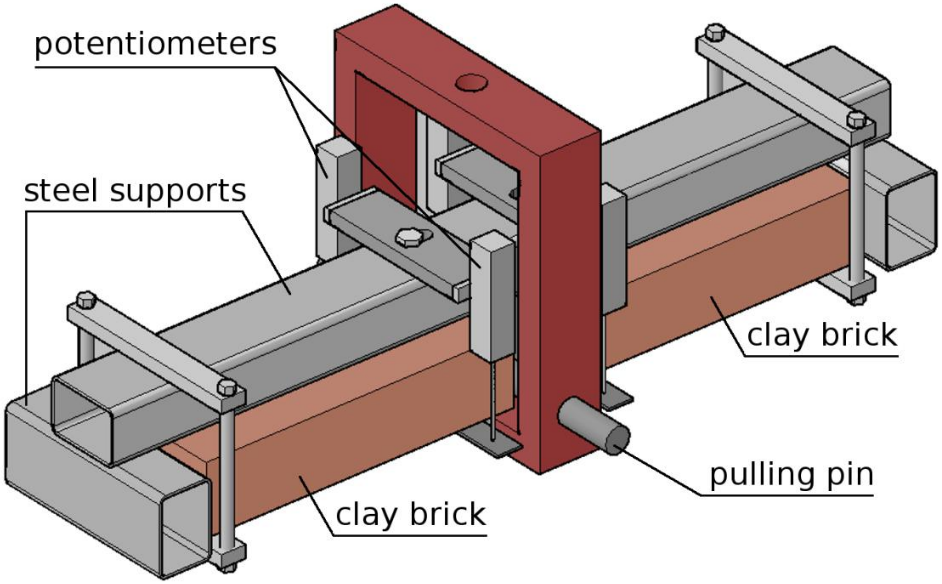

Materials and test setup

Four sets of solid clay bricks: 2 extruded and 2 facing ones.
One type of EB CFRP (high strength carbon) applied as reinforcement

Table 1: Mechanical properties of bricks

Series	f_c N/mm^2	f_f N/mm^2	f_{sp} N/mm^2	$f_{p\text{-}o}$ N/mm^2
EB1	33.3	2.97	1.34	2.75
EB2	38.4	3.89	3.51	3.02
FB1	21.1	5.29	n.a.	1.80
FB2	22.1	5.42	4.02	1.61

Table 2: Properties of reinforcement components

Adhesive MBrace® Saturant		
Charact. compr. strength	>80	N/mm^2
Charact. direct tens. strength	>50	N/mm^2
Maximum tensile strain	2.5	%
Tensile elastic modulus	>3000	N/mm^2
High-strength Carbon MBrace® C1-30		
Equivalent thickness	0.165	mm
Charact. direct tens. strength	3430	N/mm^2
Maximum tensile strain	1.5	%
Tensile elastic modulus	230000	N/mm^2

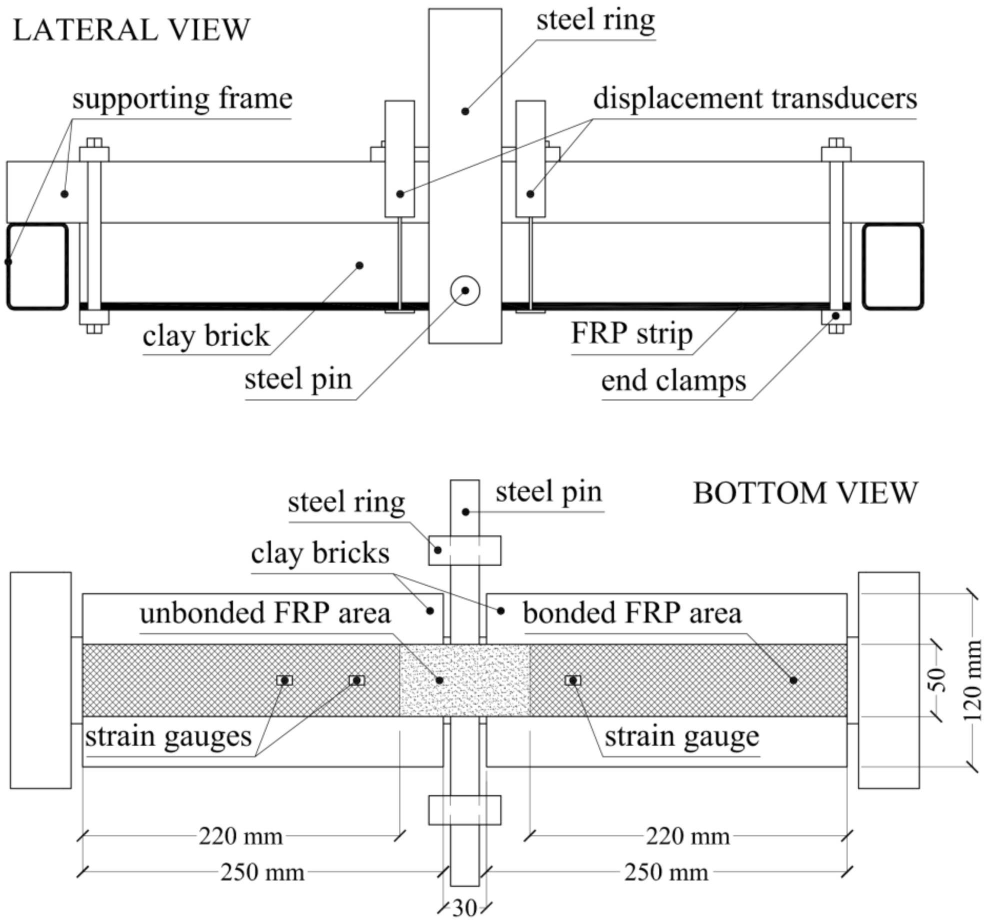

Figure 1: Design scheme of a specimen

Matteo Panizza, E. Garbin, M.R. Valluzzi, C. Modena

Test matrix and performing

Table 3: Experimental matrix of V-shape Peel Tests

Sample	brick type	loading path
VPT01 (pilot test)	FB2 - facing	monotonic (A)
VPT02 (pilot test)	EB1 - extruded	cyclic (A)
VPT03	EB1 - extruded	cyclic (A)
VPT04	FB2 - facing	cyclic (A)
VPT05	FB2 - facing	monotonic (A)
VPT06	FB2 - facing	cyclic (A)
VPT07	EB1 - extruded	cyclic (B)
VPT08	EB1 - extruded	cyclic (B)
VPT09	EB1 - extruded	monotonic (B)
VPT10	EB1 - extruded	cyclic (B)
VPT11	FB2 - facing	cyclic (B)
VPT12	EB2 - extruded	monotonic (B)
VPT13	FB1 - facing	monotonic (C)
VPT14	FB1 - facing	cyclic (C)

Table 4: Adopted test procedures

Procedure	Step	Rate mm/min	Pin direct.	Duration s
Monotonic A	1	2.0	down	up to fail.
Cyclic A	1	2.0	down	180 s
	2	2.0	up	150 s
	3	2.0	down	600 s
	4	back to step 2		
Monotonic B	1	1.0	down	up to fail.
Cyclic B	1	1.0	down	360 s
	2	2.0	up	150 s
	3	2.0	down	600 s
	4	back to step 2		
Monotonic C	1	0.6	down	up to fail.
Cyclic C	1	0.6	down	600 s
	2	1.2	up	250 s
	3	1.2	down	500 s
	4	back to step 2		

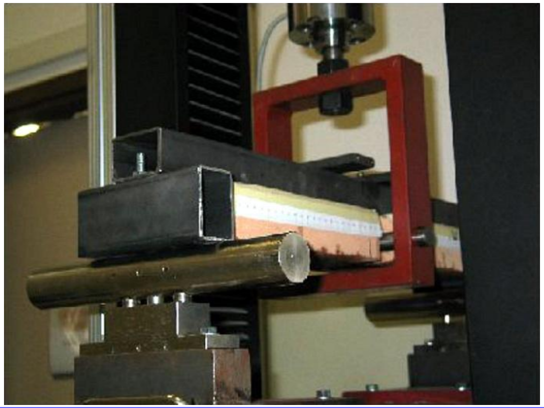

Results (1)

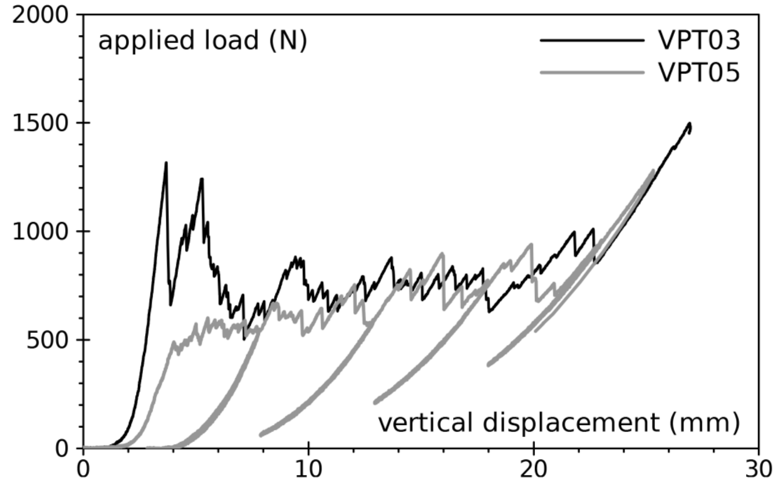

typical load-displacement curves

Example of peel angle progression

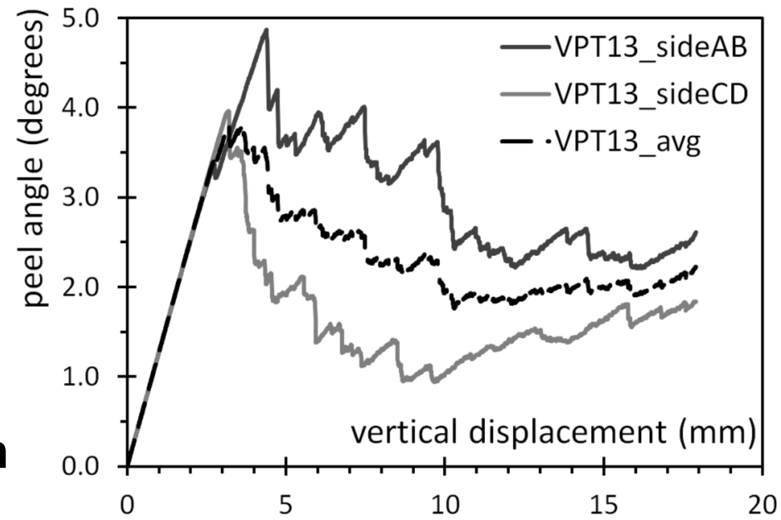

failure of extruded bricks

failure of facing bricks

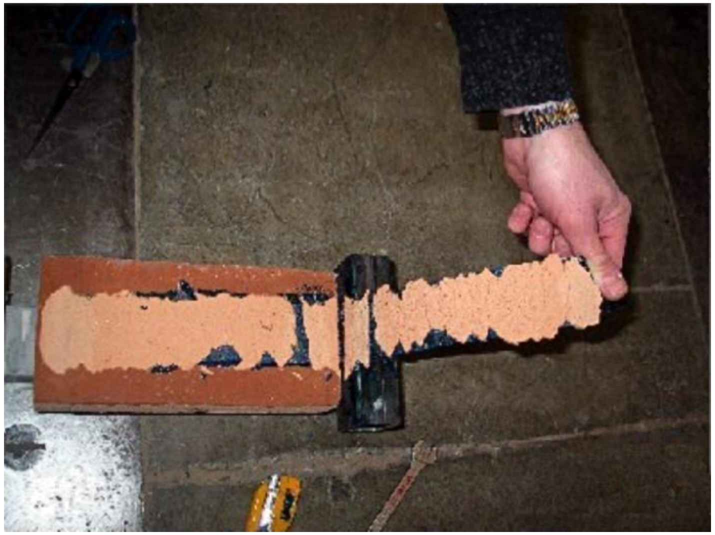

Results (2)

Brick type	Sample	P_{max} N	P_{max}/b_f N/mm	Corresp. cycle	Fail. loc.
EB1	VPT02	1308	13.1	third	I
EB1	VPT03	898	9.0	third	I+S
EB1	VPT07	765	7.7	first	I
EB1	VPT08	850	8.5	second	I
EB1	VPT09	628	6.3	-	I
EB1	VPT10	810	8.1	first	I
EB2	VPT12	940	9.4	-	I
FB1	VPT13	909	9.1	-	S
FB1	VPT14	911	9.1	first	S
FB2	VPT01	1563	15.6	-	S
FB2	VPT04	1283	12.8	second	S
FB2	VPT05	1317	13.2	-	S
FB2	VPT06	1795	18.0	first	I+S
FB2	VPT11	1241	12.4	first	I+S

maximum loads and type of failure (samples sorted by brick type) [I => "interface", S => "substrate"]

Sample	1st cycle		2nd cycle		3rd cycle	
	$\theta_{P_{max}}$ deg	θ_{avg} deg	$\theta_{P_{max}}$ deg	θ_{avg} deg	$\theta_{P_{max}}$ deg	θ_{avg} deg
VPT02	5.04	5.04	4.20	3.74	4.11	0.75
VPT03	2.87	2.87	n.a.	n.a.	n.a.	n.a.
VPT07	4.31	4.31	3.28	3.02	4.18	3.63
VPT08	5.52	5.52	5.79	4.29	5.04	4.61
VPT09	*3.62*	*3.62*				
VPT10	3.08	3.08	2.00	1.97	2.85	2.58
VPT12	*5.49*	*5.49*				
VPT13	*3.80*	*3.80*				
VPT14	4.58	4.58	3.91	3.68	3.64	3.41
VPT01	*4.40*	*4.38*				
VPT04	5.09	5.09	5.10	4.02	n.a.	n.a.
VPT05	*3.24*	*2.92*				
VPT06	4.98	4.98	4.13	2.81	2.72	2.44
VPT11	3.77	3.77	3.06	2.41	2.29	1.98

measured peel angles (samples sorted by brick type) [at max load or mean angles]

Analyses

as reported in De Lorenzis & Zavarise (2008)

$$F_0 = F\cos\theta$$

$$M_0 = \sqrt{\frac{E_f t_f^3}{6}\left[\frac{F^2\sin^2\theta}{2E_f t_f} + F\,(1-\cos\theta)\right]}$$

$$G_I = \frac{6M_0^2}{E_f t_f^3};\ G_{II} = \frac{F_0^2}{2E_f t_f};\ G = G_I + G_{II}$$

$$\psi = \arctan\sqrt{\frac{G_{II}}{G_I}} = \arctan\frac{t_f F_0}{\sqrt{12}E_f}$$

Sample	G_I N/mm	G_{II} N/mm	ψ deg	G N/mm	G_W N/mm	ΔG %
VPT02	0.472	0.436	43.9	0.908	0.344	-62%
VPT03	0.151	0.190	48.3	0.341	0.122	-64%
VPT07	0.289	0.136	34.4	0.425	0.168	-60%
VPT08	0.431	0.093	24.9	0.524	0.194	-63%
VPT09	0.199	0.129	38.9	0.329	0.129	-61%
VPT10	0.219	0.298	49.4	0.517	0.182	-65%
VPT12	0.452	0.126	27.8	0.578	0.221	-62%
VPT13	0.302	0.247	42.1	0.549	0.212	-61%
VPT14	0.365	0.171	34.4	0.536	0.212	-60%
VPT01	0.603	0.544	43.5	1.147	0.436	-62%
VPT04	0.573	0.273	34.6	0.846	0.335	-60%
VPT05	0.374	0.714	54.1	1.089	0.347	-68%
VPT06	0.784	0.560	40.2	1.344	0.524	-61%
VPT11	0.411	0.467	46.9	0.878	0.321	-63%

as reported in Wu et al. (2005) and Dai et al. (2007)

$$\begin{aligned} G_W &= E_f t_f\left(\tfrac{1}{2}\tan^2\theta + \tfrac{1}{\sqrt{1+\tan^2\theta}} - 1\right) \\ &\approx \tfrac{3}{8}E_f t_f\tan^4\theta \end{aligned}$$

$$P_{max} = E_f t_f b_f \tan^3\theta$$

$$P_{max} = 2.087 b_f G_W^{0.75}\,(E_f t_f)^{0.25}$$

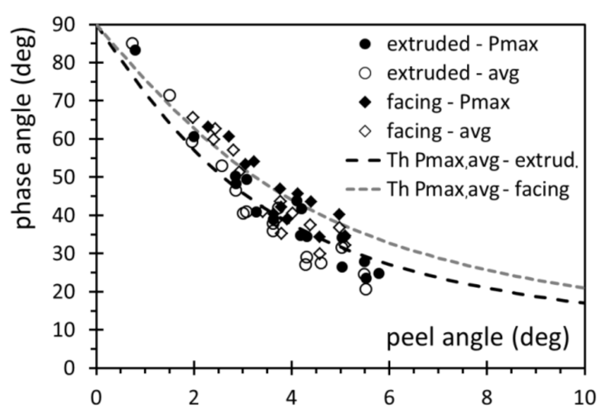

Figure 7: Phase versus peel angles

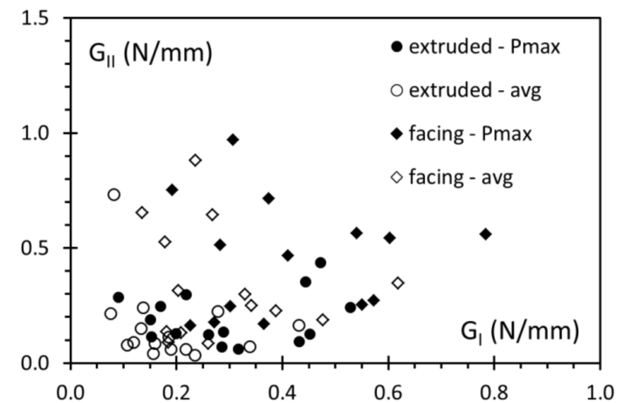

Figure 8: Evaluated mode I and II components of mixed-mode fracture energy

Conclusions

- Fourteen V-shape Peel Tests, which test set-up was based on similar tests carried out on concrete substrates, were performed using CFRP reinforcement applied to solid clay bricks. Test were aimed at investigating the possible FRP reinforcement contribution to the shear strength of thin masonry arches and vaults. Although preliminary tests, they allowed identifying the main characteristics of the investigated phenomenon.

- The experimental set-up proved to by rather feasible and adaptable to most universal test machines. Observations do not differ much from what Wu et al. (2005) and Dai et al. (2007) reported in the case of concrete substrates.

- Peel load, during the detachment, oscillated within a limited range, although scattering was in some cases very large; maximum loads of about 8–13 N/mm were observed, except for the FB2 series that resisted up to 18.8 N/mm. First peak load was generally higher than the others, for monotonic tests.

- Peel angles, similarly to peel loads, oscillated within a rather moderate range. Measured values varied in most cases between 2 and 6 degrees, however their measurement should be considered qualitative since affected by a certain imprecision and simplifying approximations.

- Calculated mixed-mode fracture energies ranged in most cases from 0.3 to 1 N/mm, hence their order of magnitude is rather consistent with values reported in literature for quasi-brittle substrates, albeit markedly affected by peel angle measurement.

THANK YOU

University of Padua – Italy

Department of Civil, Architectural and Environmental Engineering